2023-05

Entrainment and horizontal atmospheric transport of microplastics from soil

Abbasi, S

10.1016/j.chemosphere.2023.138150
Chemosphere
Elsevier BV

Entrainment and horizontal atmospheric transport of microplastics from soil

Sajjad Abbasi * [a,b], Mahrooz Rezaei [c], Monireh Mina [d], Abdolmajid Sameni [d], Patryk Oleszczuk [b], Andrew Turner [e], Coen Ritsema [f]

[a] Department of Earth Sciences, College of Science, Shiraz University, Shiraz 71454, Iran

[b] Center for Environmental Studies and Emerging Pollutants (ZISTANO), Shiraz University, Shiraz, Iran

[c] Meteorology and Air Quality Group, Wageningen University & Research, P.O. Box 47, 6700, AA, Wageningen, the Netherlands

[d] Department of Soil Science, School of Agriculture, Shiraz University, Shiraz, Iran

[e] School of Geography, Earth and Environmental Sciences, University of Plymouth, PL4 8AA, UK

[f] Soil Physics and Land Management Group, Wageningen University & Research, P.O. Box 47, 6700 AA Wageningen, the Netherlands

"Sajjad Abbasi "

Email address: sajjad.abbasi@shirazu.ac.ir; sajjad.abbasi.h@gmail.com

Scopus Author ID: https://www.scopus.com/authid/detail.uri?authorId=57203061256

Google scholar: https://scholar.google.com/citations?user=cQzmYz8AAAAJ&hl=en&oi=ao

ORCID: 0000-0002-5194-9334

https://doi.org/10.1016/j.chemosphere.2023.138150

Accepted 12 Feb 2023

Graphical Abstract

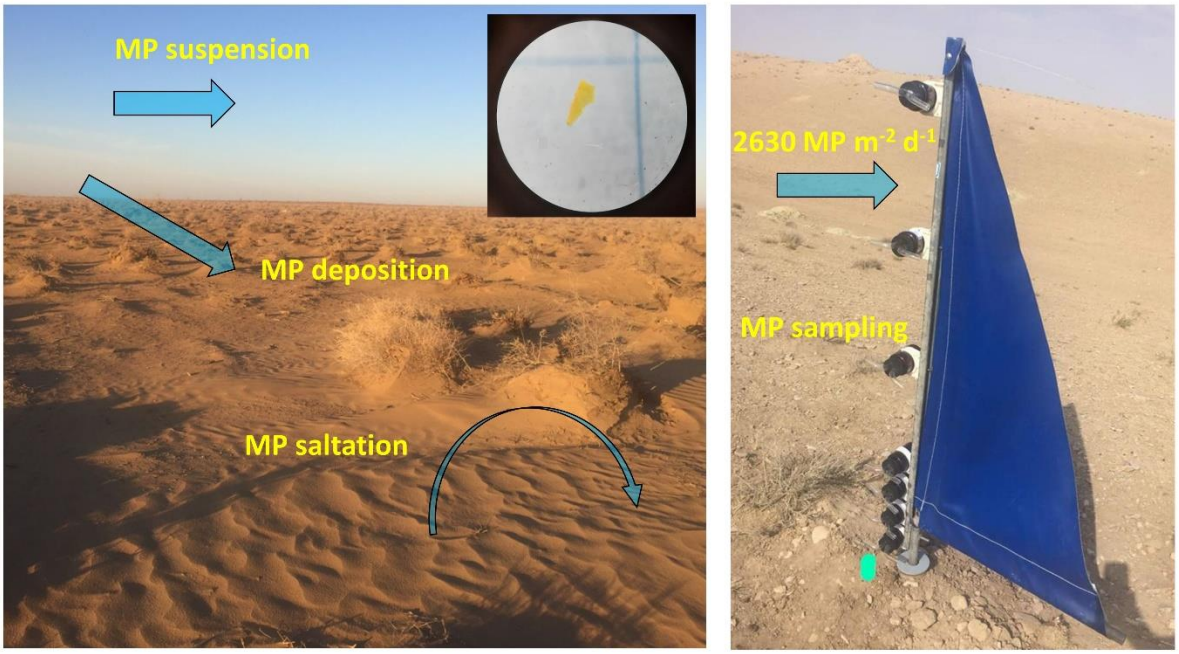

Highlights

- Horizontal sediment traps have collected microplastics (MPs) from an arid region
- Number of MPs (0 to 21) variable between sites and at different heights (up to 1 m)
- Most MPs are < 250 μm fibres of polyethylene, nylon and polypropylene
- Median vertically-averaged horizontal flux is about 2630 MP m^{-2} d^{-1}
- Observations attributed to mixing of background airborne MPs with MPs suspended from soil

Abstract

Soils are an important source of microplastics (MPs) to the atmosphere but the fluxes and mechanisms involved in MPs entrainment are not well understood. In the present study, a series of horizontally aligned sediment traps have been deployed at different heights within 1 m above the ground and for a two-month period at various locations in an arid region (Sarakhs, Iran). MPs were isolated from sediments and were quantified and characterised according to size, colour, shape and polymer composition by established techniques. Most MPs were < 250 μm in length, fibres were the most important shape, black and blue-green were the dominant colours, and polymer abundance decreased in the order polyethylene > nylon > polypropylene > polystyrene > polyethylene terephthalate. The distributions of sediment mass (range < 0.01 to 9 g) and number of MPs (range = 0 to 21) were heterogeneous, both between sites and at the different heights sampled, and yielded median, vertically-averaged horizontal fluxes for the region of about 450 g m^{-2} d^{-1} and 2600 MP m^{-2} d^{-1}, respectively. However, when data were pooled, the number of MPs normalised to sediment mass exhibited a significant inverse relationship with sediment mass, an effect attributed to the presence of ambient suspended MPs and sediment that are diluted by the suspension of soil and deposited MPs at higher wind speeds. The mechanisms of MP saltation and entrainment were not ascertained but a theoretical framework for threshold shear velocity based on regularly-shaped particles and density considerations is presented. Further experimental work is required to verify this framework, and in particular for fibrous MPs whose aerodynamic properties are very different to those of soil particles.

Keywords: Soils; Wind Erosion; Entrainment; Transport; Saltation; MWAC Sampler

1. Introduction

Although the recent literature has identified the atmosphere as a key environmental compartment for microplastics (MPs) (Wang et al., 2021; Ding et al., 2022; Evangeliou et al., 2022), little is understood about the processes controlling their inputs, transport and fate in this setting. Processes acting on MPs are likely the same as those acting on geosolids, like soils, sediments and dusts, and include saltation, entrainment, advection, horizontal conveyance, long-range transport and deposition (Kallenbach et al., 2022). However, MPs have very different properties to geosolids, with lower densities and different aspect ratios (especially for films and fibres), and consequently, different inter-particle forces and aerodynamic characteristics (Ravi et al., 2020).

Several studies have used passive sampling devices to collect, quantify and characterise MPs that have undergone dry and/or wet deposition (Cai et al., 2017; Klein and Fischer, 2019; Abbasi and Turner, 2021; Xiong et al., 2022) and have concluded that the atmosphere is instrumental to their long-range transport. Far less understood, however, is how MPs are initially entrained into the atmosphere from the terrestrial environment during wind-erosion and how MPs are subsequently transported horizontally. Empirical studies in wind tunnels deployed in the field (Rezaei et al., 2019; 2022) or in the laboratory (Bullard et al., 2021) demonstrate clear enrichment of MPs in suspended material compared with underlying soils but threshold speeds for MP suspension and horizontal MP fluxes have not been determined.

The modified Wilson and Cooke (MWAC) sediment catcher (Wilson and Cooke, 1980; Kuntze et al., 1990) consists of a vertical array of traps that allows the horizontal (including saltation) sediment mass flux to be measured and horizontal mass transport to be calculated. Accordingly, the MWAC is commonly employed in field studies of aeolian transport and wind erosion over arid and semi-arid soils (Mendez et al., 2011; Sterk et al., 2012; Webb et al., 2016). In the present study, a series of customized, 1-m modified MWAC sediment catchers have been deployed for an extended (two-month) period in an arid region subject to significant wind-erosion to capture both sediment and MPs at different heights above the ground, with MPs subsequently isolated and characterised by established methods. The spatial and vertical distributions of MPs and eroded sediments have been examined in order to better understand the nature and mechanisms of MPs entrainment and horizontal transport over soils susceptible to erosion and to explore any relationships between processes and effects acting on MPs and soils.

2. Material and Methods

2.1. Study Area

The location of Sarakhs is shown in Figure 1 along with the precise sites where sampling was undertaken. Sarakhs is a 2000 km^2 sub-basin of the Qarakhm Basin in north-east Iran that is bound to the west and south-west by the Bazangan and Shurluq mountains and to the north and east by the border with Turkmenistan (with the eastern border defined by the Harirud River). The majority of Sarakhs consists of a plain at 300 to 500 m above sea level that is subject to desertification because of an arid climate, low precipitation (annual average precipitation ~ 185 mm), unfavourable soil, land use changes, alluvial aquifer exploitation and wind erosion (Koohbanani et al., 2018; Sarbazi et al., 2020). Erosive conditions are intensified between late May and late September because of strong, persistent north-westerly to north-easterly winds (the "120-day wind") that are channelled into the region by the surrounding topography (Alizadeh-Choobari et al., 2014).

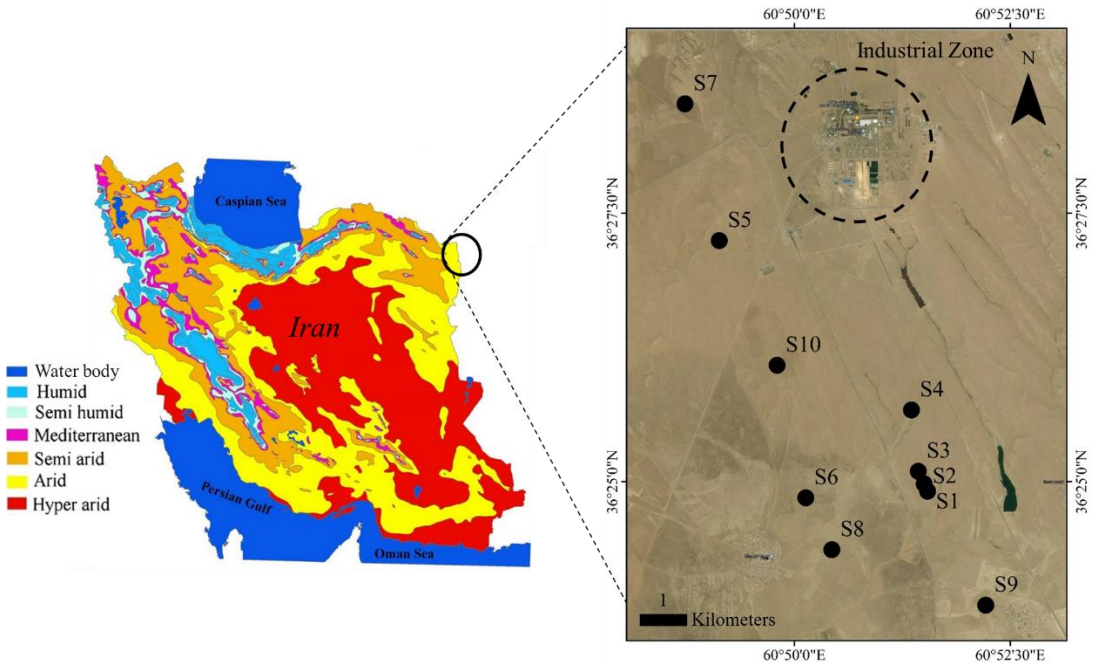

Figure 1: Location of Sarakhs and the ten sites selected for study.

2.2. Sample Collection

Airborne sediment and MPs were sampled using a series of MWAC sediment catchers deployed at ten sites in central Sarakhs (Figure 1) from 17 July 2019 to 12 September 2019 (a period of 57 days). Sampling sites included those within 5 km of an industrial zone housing oil and gas refining (S5 and S7) and those remote from any human influence (e.g., S6, S8 and S9). A wind rose defining the frequencies of wind speed and direction at a height of 10 m in Sarakhs during the study period is shown in Figure 2. Winds were predominantly northerly to north-westerly, with a maximum speed above 11 m s^{-1}, an overall average speed of about 2 m s^{-1} and calm conditions for about 30% of the time. Gravimetric analysis of 50, ~ 50 g surface soils sampled throughout the region studied and that had been mechanically fractionated through a series of stainless steel sieves as part of a parallel research project revealed the following approximate grain size distributions (mean $\pm$ one standard deviation and as percentages): > 4 mm = 5.9 $\pm$ 3.9; 2 – 4 mm = 10.2 $\pm$ 6.5; 1 – 2 mm = 9.3 $\pm$ 4.2; 0.2 - 1 mm = 20.1 $\pm$ 6.3; 0.05 – 0.2 mm = 49.4 $\pm$ 14.3; < 0.05 mm = 5.2 $\pm$ 2.2.

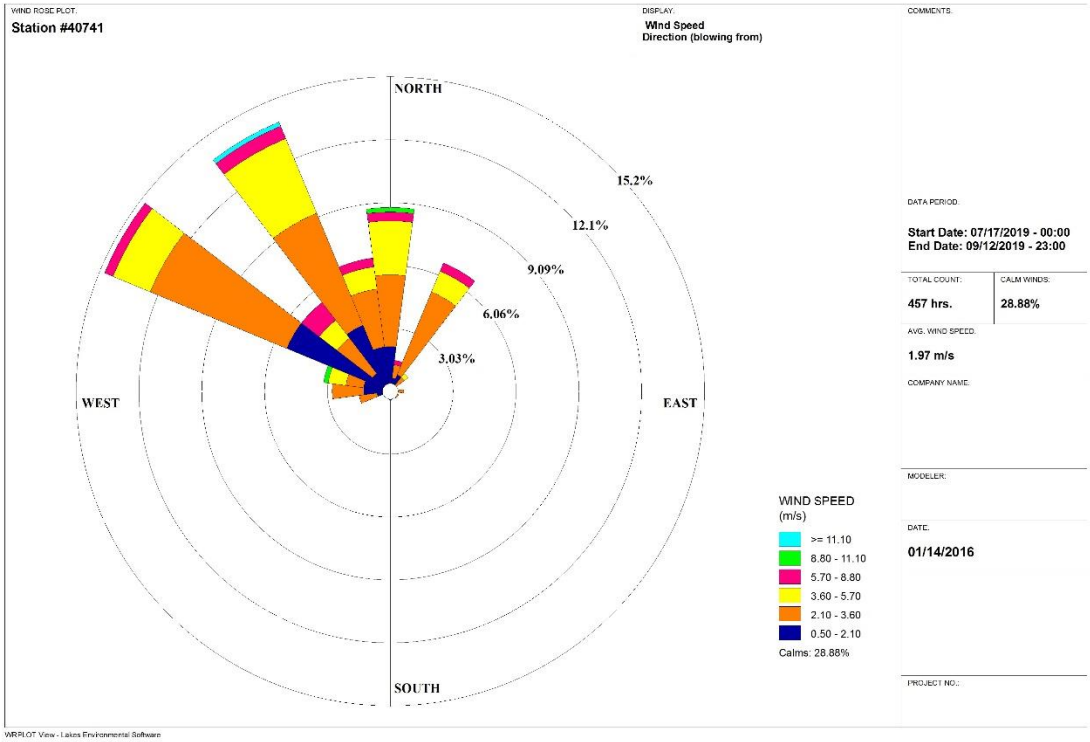

Figure 2: A wind rose for Sarakhs at a height of 10 m during the period of study.

Each MWAC sediment catcher consisted of a vertical array of seven sediment traps at heights above the ground recommended by Sterk and Raats (1996): namely, 0.05, 0.12, 0.19, 0.26, 0.50, 0.75 and 1.00 m. Traps were 100-mL amber glass bottles with 8-mm diameter glass inlet and outlet tubes that were orientated horizontally on a 1.5 m central mast. The mast was fitted with a vane that allowed the inlet tubes to face the wind, with air-borne particles that enter through the inlet tubes settling in the traps as air slows down and subsequently escapes through the outlets. MWAC sediment catchers were secured by inserting the lower 40 cm of the central pole into a metal tube that had been buried in the soil. The surrounding soil was smoothed with a metal trowel and sediment catchers were left for a period of two weeks in order to allow the disturbed terrain to acclimatise before bottles were cleaned with filtered water and dried and sampling began.

2.3. Microplastic extraction

At the end of the sampling period, bottles were wrapped in aluminium foil and transported to the laboratory. Samples were carefully transferred to pre-weighed 600-mL beakers using a stainless steel spoon and weighed on an electronic balance (Libror AEL-40SM, Shimadzu, Japan) before being sieved through a 5-mm stainless steel mesh. Each sieved sample (up to 10 g) was then weighed into a clean beaker to which 30 mL of 30% H_2O_2 (Arman Sina, Tehran) was added, with oxidation proceeding at room temperature until bubble formation ceased. Remaining particulate matter was washed with filtered, deionised water through a 150 mm diameter S&S filter paper (blue band, grade 589/3, 2 µm pore size) housed in a glass-ceramic vacuum filtration kit before being placed on an aluminium tray, covered with foil and dried in a sand bath at 60 °C for 2 h.

MPs were isolated according to Abbasi et al (2019). Briefly, dried, digested samples were transferred to 300-mL solutions of saturated $ZnCl_2$ (Arman Sina, Tehran; density 1.6 – 1.8 g cm^{-3}) in a series of clean glass beakers, and the decanted contents were subsequently centrifuged at 4000 rpm before supernatants were vacuum-filtered through S&S filter papers. Suspension, decanting and centrifugation were repeated twice before resulting filters were air-dried for 48 h at

158 25 °C in a metal cabinet and transferred to glass Petri dishes for physical and chemical
159 characterisation.

160

161 ***2.4. Microplastic identification and characterisation***

162 MPs on filters were identified and quantified under a binocular microscope (Carl-Zeiss) at 40 x to
163 200 x magnification and with the aid of ImageJ software. Identification was based on thickness
164 and cross sectional properties, shininess, hardness, surface structure and reaction to a hot, 250 µm-
165 diameter stainless steel needle. Particle size, with a lower limit of about 20 to 50 µm depending on
166 shape and colour, was estimated along the length of the longest axis, L ($L \leq 100$ µm, $100 < L \leq$
167 250 µm, $250 < L \leq 500$ µm, $500 < L \leq 1000$ µm, $L > 1000$ µm), and colour was grouped as black-
168 grey, yellow-orange, white-transparent, red-pink or blue-green. Shape was classified as film,
169 fragment, spherule-granule or fibre, with the latter defined as having a length to diameter ratio of
170 at least three.

171 The polymeric composition of all MPs isolated from sites S3 and S9 (that is, at all heights at two
172 sites where MPs were relatively abundant; $n = 88$) and an additional random 19 MPs from other
173 sites was determined using a micro-Raman spectrometer (LabRAM HR, Horiba, Japan) with a
174 laser of 785 nm, a Raman shift of 400-1800 cm^{-1} and acquisition times between 20 and 30 s.
175 Surface morphology was examined on MPs from sites S3 and S9, after they had been mounted on
176 microscope slides and gold-coated, using a high vacuum scanning electron microscope (SEM;
177 TESCAN Vega 3, Czech Republic) operated at 20 kV and with a resolution of 2 nm.

178

179 ***2.5. X-Ray diffraction analysis***

180 Sieved samples from every bottle at sites S3 and S9 were subject to X-ray diffraction (XRD)
181 analysis. Data were collected using a Bruker-D8 ADVANCE diffractometer operated in reflection
182 geometry at 40 kV and 30 mA and with a Cu-Kα source. The 2θ scan ranged from 5° to 70°, with
183 a step size of 0.02° and a counting time of 1 s, and phase identifications were conducted using the
184 X-powder software (version 2010.01.45 PRO; Martin-Islán, Granada, Spain) supported by the
185 Powder Diffraction File-2 database of the International Centre for Diffraction Data. Quantitative

X-ray diffraction analysis was performed with PROFEX software (version 3.10.2; Döbelin and Kleeberg, Bettlach, Switzerland) (Doebelin et al., 2015) and the Rietveld refinement kernel, BGMN (version 4.2.22, Netherlands Energy Research Foundation ECN, Rietveld, Petten, The Netherlands) (Bergmann et al., 1998). To evaluate the reliability of the quantitative results, the weighted-profile factor, expected R-factor and goodness of fit factor were monitored.

2.6. Quality Assurance and Quality Control

All reagents and distilled water were filtered through S&S blue band filters and kept in glass containers to prevent plastic and fibre contamination during sample processing. Operators wore white cotton laboratory coats and samples and containers were protected by aluminium foil where possible. Work surfaces were thoroughly cleaned with ethanol, glassware was cleaned with distilled water, and all windows and doors were kept closed. Analysis of five blank filters, derived from the processing of filtered water in glass bowls exposed to the same conditions as the samples, revealed no MP contamination.

As positive controls, ten polyethylene particles and ten polyvinyl chloride particles (both white and spherical and between 20 and 250 μm in diameter) were added to three glass beakers containing 500 mL of distilled water. Following digestion, isolation and identification as above, all added MPs were recovered.

2.7. Data processing and statistics

Data analysis and statistical tests were performed in Minitab *v*19. Departures from normality were identified using the Anderson-Darling test ($p > 0.95$ for normality). Non-normal data was summarised in terms of the median and lower and upper quartiles, and differences in median values were detected using a series of Kruskal-Wallis tests ($\alpha = 0.05$). Linear regressions and model calculations were performed in Excel 2013.

3. Results

The dry masses of sediment captured by the traps at each site in the Sarakhs region are shown in Table 1, along with statistical summaries based on non-normal distributions. Masses range from < 1 mg to about 9 g, and there were significant differences in median masses ($p < 0.001$) between sites. Because of the inter-site variability, however, there were no significant differences ($p > 0.05$) in median masses collected at the different heights above the ground. Moreover, there were no clear height-dependent trends in dry mass at any site, with the maximum and minimum quantities of sediment encountered at various heights amongst the different locations.

XRD analysis of samples at sites S3 and S9 revealed that the principal minerals were quartz (~ 60 to 80%), calcite (~ 5 to 21%) and albite (~ 7 to 22%), with one or more of dolomite, kaolinite and illite present below about 5%. Specific gravities, derived from the mineralogical content, ranged from 2.53 to 2.67 g cm^{-3} (mean = 2.65 g cm^{-3}) but displayed no clear differences between the two sites or with height above the ground.

Table 1: Dry masses of sediment, in g, collected by the traps at the different heights at each sampling site in the Sarakhs region over a period of 57 days. Median values and lower and upper quartiles are also shown as statistical summaries for each site and each height.

	height, m									
site	1.00	0.75	0.50	0.26	0.19	0.12	0.05	median	Q1	Q3
S1	0.49	1.01	0.10	3.75	3.67	3.22	0.92	1.01	0.71	3.45
S2	0.09	4.69	0.86	4.16	0.94	0.96	1.04	0.96	0.90	2.60
S3	0.04	3.11	1.34	1.78	1.71	0.04	1.19	1.34	0.62	1.75
S4	3.67	0.15	0.01	<0.01	0.13	0.13	0.43	0.14	0.13	0.36
S5	3.58	2.68	2.94	5.44	5.78	6.89	7.13	5.44	3.26	6.34
S6	1.27	4.75	3.21	5.28	0.26	3.02	2.47	3.02	1.87	3.98
S7	0.01	0.27	3.51	0.58	2.94	0.80	0.32	0.58	0.30	1.87
S8	4.41	4.00	4.93	4.40	4.95	5.36	4.48	4.48	4.41	4.94
S9	4.99	5.32	6.96	6.71	4.88	5.44	8.89	5.44	5.16	6.84
S10	0.43	0.24	4.99	1.20	3.14	1.26	0.64	1.20	0.54	2.20
median	0.88	2.90	3.08	4.16	3.04	2.14	1.12	2.90	1.63	3.06
Q1	0.18	0.46	0.98	1.78	1.13	0.84	0.71	0.97	0.56	1.95
Q3	3.65	4.52	4.58	5.28	4.58	4.83	3.98	4.12	2.91	4.70

The number of MPs captured by the traps at each height is shown in Table 2, along with statistical summaries based on non-normal distributions. Overall, 570 MPs were detected, with numbers in individual traps ranging from 0 to 21. There were no significant differences ($p > 0.05$) in median values between either location or height and there were no clear relationships between MP number and height. Fibres dominated MPs by shape (64.0%), with smaller contributions from fragments (26.7%), films (5.8%) and spherules (3.5%). Regarding colour, black or blue-green were most abundant (more than 30% each), with white, red-pink and yellow-orange comprising about 15%, 14% and 5%, respectively. The size distribution of MPs was skewed towards the finer fractions, with about 64% below 100 μm, 34% between 100 and 250 μm and about 2% between 250 and 500 μm; significantly, no MPs were detected above 500 μm. As with overall MPs abundance, there were no clear shifts in distributions of shape, colour or size between the different sites or as a function of height above the ground.

Table 2: Number of MPs collected by the traps at the different heights at each sampling site in the Sarakhs region over a period of 57 days. Median values and lower and upper quartiles are also shown as statistical summaries for each site and each height.

	height, m									
site	1.00	0.75	0.50	0.26	0.19	0.12	0.05	median	Q1	Q3
S1	9	6	4	5	6	11	10	6.0	5.5	9.5
S2	5	4	6	5	8	3	6	5.0	4.5	6.0
S3	9	7	5	6	6	2	7	6.0	5.5	7.0
S4	2	5	8	0	10	20	11	8.0	3.5	10.5
S5	2	7	7	8	16	12	18	8.0	7.0	14.0
S6	9	10	4	10	10	13	9	10.0	9.0	10.0
S7	5	6	5	7	7	7	16	7.0	5.5	7.0
S8	8	8	5	10	5	10	19	8.0	6.5	10.0
S9	5	2	14	10	3	6	6	6.0	4.0	8.0
S10	11	4	10	10	9	21	20	10.0	9.5	15.5
median	6.5	6.0	5.5	7.5	7.5	10.5	10.5	7.5	6.3	9.0
Q1	5.0	4.3	5.0	5.3	6.0	6.3	7.5	6.0	4.8	7.3
Q3	9.0	7.0	7.8	10.0	9.8	12.8	17.5	8.0	6.9	10.4

The number of MPs detected normalised to the quantity of sediment captured is shown for each site and height in Table 3, along with statistical summaries based on non-normal distributions. Values range from 0 to 800 MP g^{-1} overall, and vary widely both between and within sites, with maximum and minimum values occurring at different heights among the different sites. There were significant differences ($p < 0.05$) in median values between sites but not between different heights.

Table 3: Number of MPs per g of sediment collected by the traps at the different heights at each sampling site in the Sarakhs region over a period of 57 days. Median values and lower and upper quartiles are also shown as statistical summaries for each site and each height.

	height, m									
site	1.00	0.75	0.50	0.26	0.19	0.12	0.05	median	Q1	Q3
S1	18.4	5.9	40.0	1.3	1.6	3.4	10.9	5.9	2.5	14.6
S2	55.6	0.9	7.0	1.2	8.5	3.1	5.8	5.8	2.2	7.7
S3	225.0	2.3	3.7	3.4	3.5	50.0	5.9	3.7	3.4	27.9
S4	0.5	33.3	800.0	0.0	76.9	153.8	25.6	33.3	13.1	115.4
S5	0.6	2.6	2.4	1.5	2.8	1.7	2.5	2.4	1.6	2.6
S6	7.1	2.1	1.2	1.9	38.5	4.3	3.6	3.6	2.0	5.7
S7	500.0	22.2	1.4	12.1	2.4	8.8	50.0	12.1	5.6	36.1
S8	1.8	2.0	1.0	2.3	1.0	1.9	4.2	1.9	1.4	2.1
S9	1.0	0.4	2.0	1.5	0.6	1.1	0.7	1.0	0.6	1.3
S10	25.6	16.7	2.0	8.3	2.9	16.7	31.3	16.7	5.6	21.1
median	12.7	2.4	2.2	1.7	2.8	3.9	5.8	2.8	2.3	4.8
Q1	1.2	2.0	1.6	1.4	1.8	2.2	3.8	2.7	1.7	3.4
Q3	48.1	14.0	6.2	3.1	7.3	14.7	21.9	10.5	5.0	26.2

A summary of the results arising from Raman analysis is shown in Figure 3. Of 107 samples isolated from sites 3 and 9 and from a selection of other sites and heights, 102 were petroleum-based plastics, one was a natural or synthetic rubber (polyisoprene), one was a mineral-based particle (subsequently neglected) and three returned a match with the additive, polyethylene oxide. More than one-half of the samples were constructed of polyethylene, nylon and polypropylene, and fibres were the most important shape amongst these polymers and polyphenylsulfone. Fragments were the most abundant shape amongst the remaining polymers and films were observed in MPs constructed of polyethylene, nylon, polystyrene and polyethylene terephthalate while spherules were observed in MPs constructed of polyethylene, nylon and polystyrene. Regarding sites 3 and 9, there was no dependency of MP polymer on height above ground, with both low-density polymers (< 1 g cm^{-3}; polyethylene and polypropylene) and high-density polymers (> 1.2 g cm^{-3}; polyvinyl chloride, polyethylene terephthalate, polyphenylsulfone) distributed throughout the different heights sampled.

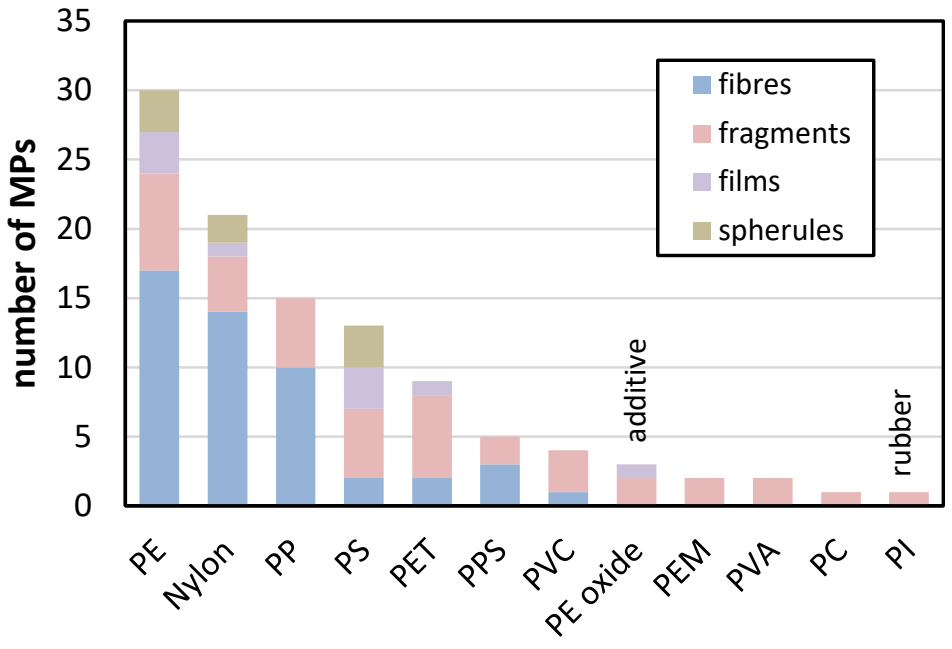

Figure 3: MPs captured in the Sarakhs region (*n* = 106, and including a rubber and three "additives") shown in descending order of polymer abundance and classified by shape. PE =

279 polyethylene; PP = polypropylene; PS = polystyrene; PET = polyethylene terephthalate; PPS =
280 polyphenylsulfone; PVC = polyvinyl chloride; PE oxide = poly(ethylene oxide); PEM = poly(ethyl
281 methacrylate); PVA = poly(vinyl alcohol); PC = polycarbonate; PI = polyisoprene.

282

283 **4. Discussion**

284 The distributions of sediment mass captured by the MWAC devices in the Sarakhs region are
285 heterogeneous both between sites and, for a given site, between the different heights sampled. The
286 deployment of MWAC catchers in the short-term or for a single event, for example, is expected to
287 return an exponential, logarithmic or power reduction in sediment mass with increasing height
288 (Dong et al., 2003; Namikas, 2003). In the present study, however, we required deployment over
289 an extended period, covering multiple events or processes (e.g., dust storms and streamers) of
290 different intensities and from different wind directions, to capture sufficient material for reliable
291 MPs isolation. MPs sampled by the MWAC sediment catchers are also heterogeneously distributed
292 on a number basis, and both spatially and as a function of height. This heterogeneity encompasses
293 the number of particles and the number normalised to sediment mass, as well as measures of size,
294 colour, shape and polymeric construction.

295 Because data could not be fitted with regression curves as a function of height, it was not possible
296 to determine vertically integrated horizontal fluxes. However, the net, vertically averaged
297 horizontal fluxes of sediment and MPs within 1 m of the ground in the Sarakhs region may be
298 estimated from the median sediment masses and MP numbers at each site captured through an inlet
299 aperture of 50 mm^2 and over a deployment period of 57 days. Fluxes, shown in Table 4, range
300 from 49 to 1908 g m^{-2} d^{-1} for sediment, with a median of about 450 g m^{-2} d^{-1}, and from 1754 to
301 3509 MP m^{-2} d^{-1}, with a median of about 2600 MP m^{-2} d^{-1}. We did not determine vertical,
302 depositional fluxes of sediment or MPs in the present study. However, Abbasi and Turner (2021)
303 measured the monthly dry depositional fluxes of sediment (dust) and MPs over a remote and
304 urbanised region of south-western Iran at a height of a few m above the ground. For the period of
305 July to September, remote and urban mean daily fluxes were about 0.5 and 3 g of sediment m^{-2}
306 and 15 and 100 MP m^{-2}. More widely, depositional rates in both urban and more remote areas are
307 typically on the order of several hundred MP m^{-2} d^{-1} (Cai et al., 2017; Zhou et al., 2017; Allen et
308 al., 2019; Klein and Fischer, 2019). Clearly, therefore, it would appear that the horizontal fluxes

of MPs (and sediment) within 1 m of the surface are considerably greater than vertical depositional fluxes.

Table 4: Vertically averaged (median) horizontal sediment and MP fluxes for the ten sites in the Sarakhs region.

site	sediment, g m^{-2} d^{-1}	MP m^{-2} d^{-1}
S1	354	2105
S2	337	1754
S3	470	2105
S4	49	3157
S5	1909	2807
S6	1060	3509
S7	204	2456
S8	1571	2807
S9	1909	2105
S10	421	3509
median	446	2632
Q1	341	2105
Q3	1443	3070

Despite the spatial and vertical heterogeneity of sediment and MP distributions noted above, when all data are pooled together distinctive relationships between the sediment mass-normalised number of MPs and sediment mass are evident. Figure 4 shows these relationships for all MPs and for fibrous MPs, along with the corresponding best-fit power-law equations of the form: $y = ax^{-b}$; where a and b are empirical constants. Here, the x-axis might be considered as a scale of the wind-speed or energy available for suspension-resuspension and transport of material. Thus, conditions of low energy are able to readily suspend and transport a relatively high proportion of fine, low density MPs but a low proportion of denser sediment grains, while conditions of high energy are able to suspend and transport greater quantities (and, presumably, sizes) of more local sediment that act to dilute the less variable suspended MP stock. According to the equations of best fit, values defining the respective "ambient" and "diluent" end-members (at sediment masses of 10 mg and 10 g, respectively) are about 660 MP g^{-1} and 0.74 MP g^{-1} and 505 MP fibres g^{-1} and 0.44 MP fibres g^{-1}.

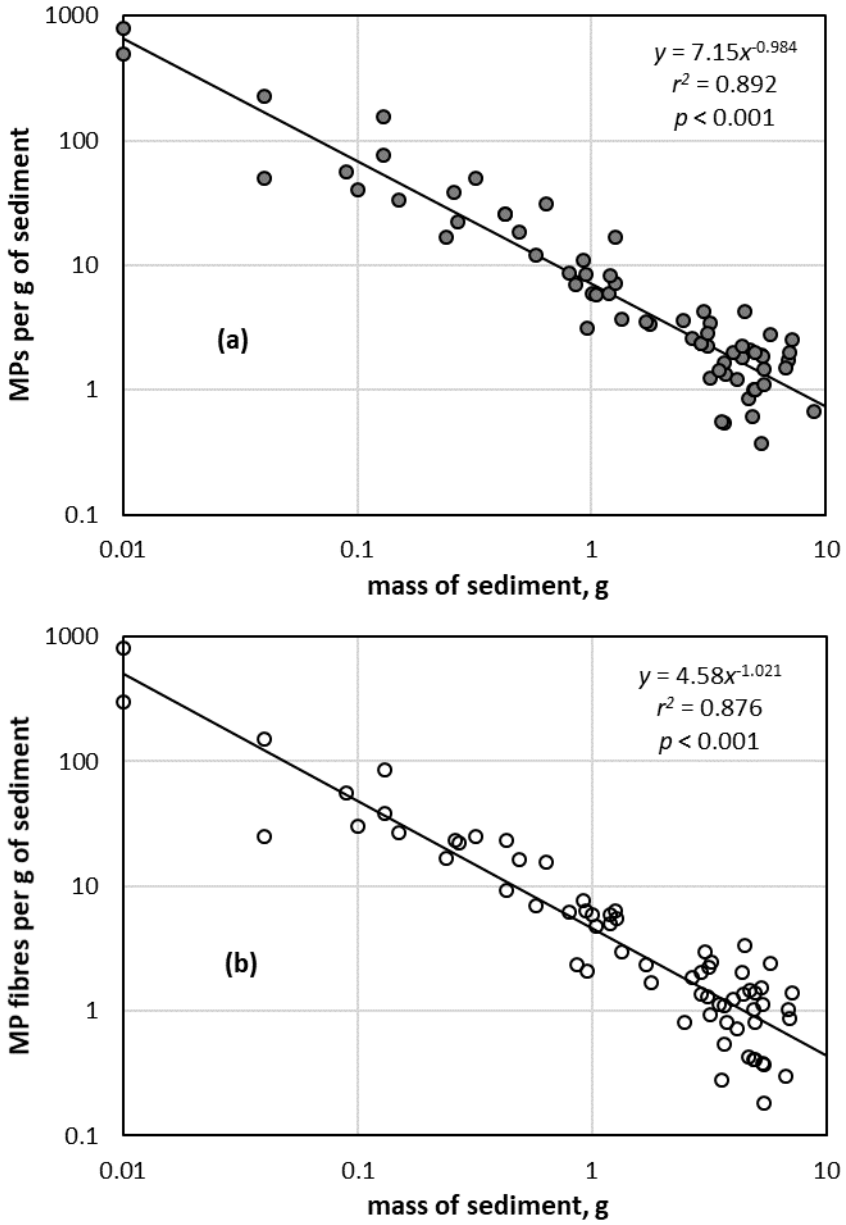

Figure 4: Numbers of (a) MPs per g of sediment and (b) MP fibres per g of sediment versus mass of sediment for all samples collected in the Sarakhs region.

The data obtained in the present study allow us to make some inferences and estimates about the mode of particle transport. Thus, under a typical range of conditions and according to Hudson (1982), sediment particles of density ~ 2.5 g cm^{-3} subject to creep have diameters ranging from 0.5 to 2 mm, those subject to saltation range from 0.05 to 0.5 mm, and those smaller than 0.1 mm are suspended (but without saltation), with overlap arising because of differences in particle density, wind speed and sediment texture. In addition, particles in the finest category may be suspended in the short-term (20 to 100 μm) or long-term (< 20 μm) (Kok et al., 2012). Based on the surface particle size data for Sarakhs reported above (Section 2.2) we predict that, on average, 5 to 10% of soil could be transported (as sediment) by creep, up to 70% could be transported by saltation and up to 50% could become suspended. The configuration of the MWAC sediment catchers does not allow us to estimate creep but the (variable) mass of material retained by the lowest sediment trap suggests that between < 1 and 80% of soil may have been transported by saltation close to the ground (~ 50 mm) while the remaining mass retained suggests that between 20% and > 99% may have been transported in suspension.

The relative modes of transport of MPs are very different to those of soil particles. Discrepancies arise because of the lower densities of MPs (~ 0.9 to 1.4 g cm^{-3} for the polymers illustrated in Figure 3) and consequent lower gravitational pulls, their smaller diameters or lengths (mostly below 200 μm) and, particularly for thin films and fibres with high aspect ratios, very different aerodynamic properties. Although the precise mechanisms and thresholds for MP emissions from soil are unknown, suggestions have been put forward based on theoretical considerations or observations of other low-density particles.

Shao and Lu (2000) and Ravi et al. (2020) provide a semi-empirical expression for the saltation threshold shear velocity, u_{*t}, based on particle density, ρ_p, and particle diameter, D_p:

$$u_{*t} = A_N \sqrt{\frac{\rho_p - \rho_a}{\rho_a} g D_p + \frac{\gamma}{\rho_a D_p}}$$

Equation 1

where ρ_a is the density of air, g is the acceleration due to gravity, A_N is a dimensionless parameter and γ is a parameter that accounts for the strength of inter-particle forces. Figure 5 shows values

of u_{*t} as a function of D_p between 50 μm and 2 mm for particles of density 2.65 g cm^{-3}, the mean value obtained from our XRD analyses of sediments, 0.9 g cm^{-3}, representative of low density polymers observed in Sarakhs like polypropylene, and 1.4 g cm^{-3} representative of higher density polymers observed in the region like PET or PVC. Note that shape is constant amongst the different densities and we used the default values for A_N (= 0.11) and γ (= 2.9×10^{-4} N m^{-1}) reported by Ravi et al. (2020) and an air density of 1.225 kg m^{-3}.

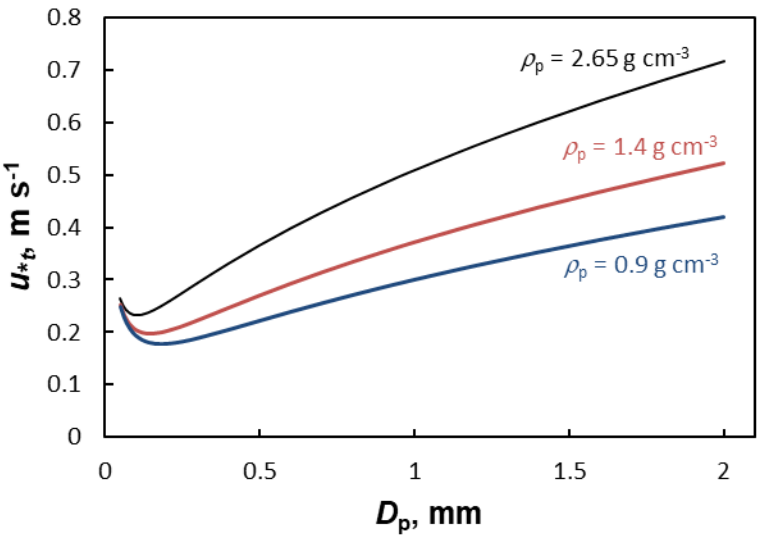

Figure 6: Saltation threshold shear velocity, u_{*t}, as a function of particle diameter, D_p, for three different particle densities, ρ_p, calculated according to equation 1.

For a given particle density, u_{*t} decreases with decreasing D_p until a point of inflection where inter-particle cohesion becomes increasingly important (the second term on the right-hand side of equation 1). For a given particle diameter, decreasing ρ_p is accompanied by decreasing u_{*t} but the magnitude of any difference decreases with decreasing particle diameter. This means that the difference between shear forces required to suspend soils and MPs diminishes with decreasing particle size such that below about 50 μm, they are similar. In other words, at low wind speeds, small soil particles and MPs of similar diameters can be entrained but at higher wind speeds MPs larger than soil particles are subject to suspension.

The framework above provides a general understanding of the suspension of regularly-shaped MPs based on density considerations. Moreover, it is qualitatively consistent with the observations made in our study (see Figure 4) and with the enrichment of MPs in eroded sediments compared with soils in wind tunnel experiments or other passive capturing devices deployed over different land-uses (Rezaei et al., 2019; 2022; Tian et al., 2022). However, additional effects may be present when MPs and soil particles co-exist and for MPs that have different shapes and aerodynamic diameters. For instance, Koutnik et al. (2021) argue that, in addition to the direct emission from soil surfaces, entrainment of MPs by wind may also proceed via bombardment of saltating soil particles close to the surface and though the disintegration of large particles or aggregates where plastics may be trapped. By contrast, and because of their lower densities, it is unlikely that saltating MPs have sufficient energy to eject mineral particles. Spherical MPs in particular are also susceptible to migration and burial in heterogeneous soils through armouring and winnowing effects, providing a means by which microbeads may be retained in this environment (Bullard et al., 2021) and accounting for the relatively low abundance of regularly-shaped MPs captured in the present study.

Fibrous MPs are less like soil particles because of their greater aspect ratios. For instance, the ratio for natural mineral particles is typically around 1.5 (Ginoux, 2003), whereas ratios for fibrous MPs may be in the hundreds (Abbasi et al., 2022). Wind tunnel experiments have revealed that 5-mm polyester fibres are more easily entrained than ~200-250 μm diameter polyethylene beads from soil and sand (Bullard et al., 2021), and once entrained fibres have lower settling velocities because of their higher surface area to volume ratio and opposing fluid drag relative to gravitational pull (Brahney et al., 2020). Fibres are also less susceptible to burial in soils than regularly-shaped MPs like spherules because of their shape and pliability (Bullard et al., 2021).

While it is important to understand the mechanisms behind the emission of MPs from soil, it must be appreciated that this environment represents a secondary MP source that acts to redistribute and, potentially, modify material. Thus, the very presence of MPs in a remote region like Sarakhs, where no plastic-based mulch or fertiliser has been applied, requires the long-range transport of MPs in suspension from various primary sources (Allen et al., 2019; Bergmann et al., 2019; Zhang et al., 2019; Brahney et al., 2020). The wind rose data in Figure 2 suggest that any primary regional sources of MPs in this study are likely to be located to the north or north-west of Sarakhs.

5. Conclusions

The present study has shown that the near-surface (< 1 m) distributions of airborne sediments and MPs captured by vertical arrays of horizontal traps in an arid region are heterogeneous, both spatially and as a function of height above the ground and, for MPs, with respect to colour, shape and polymeric composition. Consequently, estimated vertically-averaged horizontal fluxes of sediment and MPs are variable, ranging from 49 to 1909 g m^{-2} d^{-1} (median = 446 g m^{-2} d^{-1}) and 1754 to 3509 MP m^{-2} d^{-1} (median = 2632 MP m^{-2} d^{-1}), respectively. Data pooled from all traps, however, results in a significant inverse relationship between MPs normalised to sediment mass as a function of sediment mass suggesting that a background elevated in MPs relative to fine sediment is diluted by the entrainment of material containing lower quantities of MPs relative to coarser sediment. While these observations, coupled with theoretical considerations, indicate that MPs are more readily suspended and transported than soil particles, further controlled studies are required to elucidate the precise mechanisms responsible.

Acknowledgements

We thank Shiraz University for financial and technical support

444

References

Abbasi, S., Keshavarzi, B., Moore, F., Turner, A., Kelly, F.J., Dominguez, A.O., Jaafarzadeh, N., 2019. Distribution and potential health impacts of microplastics and microrubbers in air and street dusts from Asaluyeh County, Iran. Environmental Pollution 244, 153-164.

Abbasi, S., Turner, A., 2021. Dry and wet deposition of microplastics in a semi-arid region (Shiraz, Iran). Science of the Total Environment 786, 147358.

Abbasi, S., Rezaei, M., Ahmadi, F., Turner, A., 2022. Atmospheric transport of microplastics during a dust storm. Chemosphere 292, 133456.

Alizadeh-Choobari, O., Zawar-Reza, P., Sturman, A., 2014. The "wind of 120 days" and dust storm activity over the Sistan Basin. Atmospheric Research 143, 328-341.

Allen, S., Allen, D., Phoenix, V.R., Le Roux, G., Jimenez, P.D., Simonneau, A., Binet, S., Galop, D., 2019. Atmospheric transport and deposition of microplastics in a remote mountain catchment. Nature Geoscience 12, 339-344.

Bergmann, M., Mützel, S., Primpke, S., Tekman, M.B., Trachsel, J., Gerdts, G., 2019. White and wonderful? Microplastics prevail in snow from the Alps to the Arctic. Scientific Advances 5, eaax1157.

Brahney, J., Hallerud, M., Heim, E., Hahnenberger, M., Sukumaran, S., 2020. Plastic rain in protected areas of the United States. Science 368, 1257-1260.

Cai, L., Wang, J., Peng, J., Tan, Z., Zhan, Z., Tan, X., Chen, Q., 2017. Characteristic of microplastics in the atmospheric fallout from Dongguan city, China: preliminary research and first evidence. Environ. Sci. Pollut. Res. 24, 24928–24935.

Ding, J., Sun, C., He, C., Zheng, L., Dai, D., Li, F., 2022. Atmospheric microplastics in the Northwestern Pacific Ocean: Distribution, source, and deposition. Science of the Total Environment 829, 154337.

Dong, Z., Liu, X., Wang, H., Zhao, A., Wang, X., 2003. The flux profile of a blowing sand cloud: a wind tunnel investigation. Geomorphology 49, 219–230.

Evangeliou, N., Tichy, O., Eckhardt, S., Zwaaftink, C.G., Brahney, J., 2022. Sources and fate of atmospheric microplastics revealed from inverse and dispersion modelling: From global emissions to deposition. Journal of Hazardous Materials 432, 128585.

Ginoux, P., 2003. Effects of nonsphericity on mineral dust modelling. Journal of Geophysical Research 108 (D2), 4052.

Hudson, N., 1982. Soil Conservation. Batsford Ltd., London.

Kallenbach, E.M.F., Rødland, E.S., Buenaventura, N.T., Hurley, R., 2022. Microplastics in terrestrial and freshwater environments. In: Bank, M.S., ed, Microplastic in the Environment: Pattern and Process. Springer Nature, Cham, Switzerland, pp.87-130

Klein, M., Fischer, E.K., 2019. Microplastic abundance in atmospheric deposition within the Metropolitan area of Hamburg, Germany. Sci. Total Environ. 685, 96–103.

Kok, J. F., Parteli, E. J. R., Michaels, T. I., Karam, D. B., 2012. The physics of wind-blown sand and dust. Reports on Progress in Physics 75, 106901.

Koohbanani, H., Barati, R., Yazdani, M., Sakhdari, S., Jomemanzari, R., 2018. Groundwater recharge by selection of suitable sites for underground dams using a GIS-based fuzzy approach in semi-arid regions. In: Progress in River Engineering & Hydraulic Structures, International Energy and Environment Foundation, pp.11-32.

Koutnik, V.S., Leonard, J., Alkidim, S., DePrima, F.J., Ravi, S., Hoek, E.M.V., Mohanty, S.K., 2021. Distribution of microplastics in soil and freshwater environments: Global analysis and framework for transport modeling. Environmental Pollution 274, 116552.

Kuntze, H., Beinhauer, R., Tetzlaff, G., 1990. Quantification of soil erosion by wind, I. Final report of the BMFT project. University of Hannover (in German).

Mendez, M.J., Funk, R., Buschiazzo, D.E., 2011. Field wind erosion measurements with Big Spring Number Eight (BSNE) and Modified Wilson and Cook (MWAC) samplers. Geomorphology 129, 43-48.

Namikas, S.L., 2003. Field measurement and numerical modelling of Aeolian mass flux distributions on a sandy beach. Sedimentology 50, 303–326.

Ravi, S., Li, J., Meng, Z., Zhang, J., Mohanty, S., 2020. Generation, resuspension, and transport of particulate matter from biochar-amended soils: A potential health risk. GeoHealth 4, e2020GH000311.

Rezaei, M., Riksen, M.J.P.N., Sirjani, E., Sameni, A., Geissen, V. 2019. Wind erosion as a driver for transport of light density microplastics. Science of the Total Environment 669, 273-281.

Rezaei, M., Abbasi, S., Pourmahmood, H., Oleszczuk, P., Ritsema, C., Turner, A., 2022. Microplastics in agricultural soils from a semi-arid region and their transport by wind erosion. Environmental Research 212, 113213.

Sarbazi, M., Ownegh, M., Behbahani, A.M., Akbari, M., 2020. Evaluating and Modeling Temporal-Spatial Changes of Land Use in the Expansion of Desertification Intensity in the Arid Regions of Northeast Iran (Sarakhs). Geography and Environmental Hazards 34, 1-6.

Shao, Y., Lu, H., 2000. A simple expression for wind erosion threshold friction velocity. Journal of Geophysical Research 105(D17), 22437–22443.

Sterk, G., Raats, P.A.C., 1996. Comparison of models describing the vertical distribution of wind-eroded sediment. Soil Science Society of America Journal 60, 1914-1919.

Sterk, G., Parigiani, J., Cittadini, E., Peters, P., Scholberg, J., Peri, P., 2012. Aeolian sediment mass fluxes on a sandy soil in Central Patagonia. Catena 95, 112-123.

Tian, X., Yang, M., Guo, Z., Chang, C., Li, J., Guo, Z., Wang, R., Li, Q., Zou, X., 2022. Plastic mulch film induced soil microplastic enrichment and its impact on wind-blown sand and dust. Science of the Total Environment 813, 152490.

Wang, X.H., Liu, K., Zhu, L.X., Li, C.J., Song, Z.Y., Li, D.J., 2021. Efficient transport of atmospheric microplastics onto the continent via the East Asian summer monsoon. Journal of Hazardous Materials 414, 125477.

Webb, N.P., Galloza, M.S., Zobeck, T.M., Herrick, J.E., 2016. Threshold wind velocity dynamics as a driver of aeolian sediment mass flux. Aeolian Research 20, 45-58.

Wilson, S.J., Cooke, R.U., 1980. Wind erosion. In: M.J. Kirkby and R.P.C. Morgan (eds.) Soil Erosion. John Wiley & Sons, Chichester, UK. pp. 217-251.

Xiong, X., Tappenbeck, T.H., Wu, C.X., Elser, J.J., 2022. Microplastics in Flathead Lake, a large oligotrophic mountain lake in the USA. Environmental Pollution 306, 119445.

Zhang, Y., Gao, T., Kang, S., Sillanpaa, M., 2019. Importance of atmospheric transport for microplastics deposited in remote areas. Environ. Pollut. 24, 112953.

Zhou, Q., Tian, C., Luo, Y., 2017. Various forms and deposition fluxes of microplastics identified in the coastal urban atmosphere. Chin. Sci. Bull. 62, 3902–3909.